ACS Sustainable Chemistry & Engineering

pubs.acs.org/journal/ascecg

Research Article

Deciphering Redox Pathways in Aqueous Microdroplets: Simultaneous Production of Hydrogen Peroxide, Hydrogen, and Organics from Ethyl Palmitate as Renewable Feedstock

Sonam Rani, Hung V. Nguyen, Lingyang Zhu, Supriya Das, Charles M. Schroeder,[¶] and Joaquín Rodríguez-López*

Cite This: *ACS Sustain. Chem. Eng.* 2026, 14, 15850−15862

Read Online

ACCESS | Metrics & More | Article Recommendations | Supporting Information

ABSTRACT: Ultrasonication of biphasic mixtures involving water and oil forms water microdroplets, offering a promising platform that spontaneously generates hydrogen peroxide and hydrogen gas. However, the redox mechanisms underpinning these transformations are poorly understood, and most existing studies rely heavily on petroleum-derived alkanes like hexadecane. Herein, we introduce a sustainable alternative by utilizing ethyl palmitate, a renewable and plant-based oil as the organic phase. We move beyond the reactive microdroplet narrative to provide a mechanistic framework that captures redox transformations in sonicated emulsive water microdroplets (SEWMs). We demonstrate the catalyst-free production of hydrogen peroxide (∼12 mM) and hydrogen gas (∼0.75 μmol) via reduction and simultaneous oxidation of ethyl palmitate into value-added organic products (generating millimolar amounts of methanol, ethanol, methanediol, oxydimethanol, formic acid, and acetic acid), thus completing a redox coupled process within the microdroplet environment. Bright-field microscopy imaging analyses reveal that increased droplet populations and decreased droplet size correlate with higher reactivity. Furthermore, H_2O_2 and H_2 formation exhibits anticorrelated trends, indicating competing interfacial reaction pathways and tunable product selectivity by varying the gaseous environment during ultrasonication. Together, these findings expand microdroplet chemistry to plant-based oil systems and highlight SEWMs as a renewable platform for sustainable redox chemical transformations.

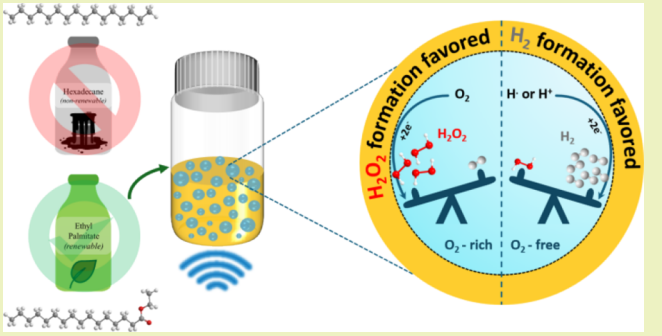

KEYWORDS: *sonicated emulsive water microdroplets, biphasic system, catalyst-free synthesis, sacrificial electron donor, redox balance*

INTRODUCTION

Generating chemicals through redox reactions using renewable sources, such as water, air, and biofeedstocks, is an attractive strategy for decarbonizing the chemical industry.[1−5] This shift allows for the reinvestigation of novel synthetic pathways that minimize hazardous chemical utilization and explore alternative energy inputs. The urgent need for such decentralized technologies is best illustrated by the current production methods of hydrogen peroxide (H_2O_2) and hydrogen gas (H_2). Currently, H_2O_2 is produced almost exclusively (>95%) by the centralized anthraquinone auto-oxidation (AO) process,[6] a capital-intensive process that relies on hazardous organic solvents and energy-intensive separations.[7] These constraints make on-site H_2O_2 production nonfeasible in many applications. On the other hand, H_2 is considered to be a promising clean fuel[8,9] but is predominantly produced by the steam methane reforming process,[10] which is a fossil-based and CO_2-intensive process[11] that accounts for ∼95% of global H_2 supply. Consequently, new approaches capable of generating both H_2O_2 and H_2 from abundant biofeedstocks are of interest for sustainable process development.

Among the emerging technologies, the unique chemistry occurring at the water microdroplet interface has garnered significant attention as a transformative platform for catalyst-free chemical synthesis.[12] Aqueous microdroplets, whether generated via electrospray, nebulization, or ultrasonication, can enable or accelerate the rate of certain chemical reactions by several orders of magnitude compared to the same reactions in the bulk.[13−19] This phenomenon is largely attributed to microdroplets' high interfacial area, intrinsic electric fields

Received: May 17, 2026
Revised: August 15, 2026
Accepted: August 20, 2026
Published: August 27, 2026

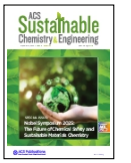

formed at their interfaces, excess charge, and contact electrification.[20−22] The synergy of two or more of these features could promote the formation of reactive oxygen species (ROS) such as H_2O_2 and highly oxidizing radical intermediates such as the hydroxyl radical, ·OH.[20,22−24] Recently, we reported that the ultrasonication of water-in-hexadecane emulsions, generating sonicated emulsive water microdroplets (SEWMs), enables the spontaneous reduction of O_2 in air to produce H_2O_2 at mM concentrations.[23] Despite the formation of highly oxidising ROS, this work showed that conditions within SEWMs are reductive, capable of producing both H_2O_2 through the oxygen reduction reaction (ORR) and also hydrogen gas (H_2).[23] The microenvironment within SEWMs resulting from confinement in a droplet, redox, and sonochemical excitation can be exploited for complex redox reactions such as biopolymer deconstruction to valorized products,[25] opening new avenues for analogous reaction classes encountered with sprayed microdroplets, e.g., in the production of urea, uracil, and complex inorganic materials.[26−29] However, elucidating the origin of the redox pathways and the role that the oil plays in SEWMs is necessary to advance this field of research.

A fundamental aspect of redox transformations is the need for an electron donor and an acceptor to complete the reactive cycle. This requirement has led to significant discussion in the microdroplet community about the origin of redox intermediates and products at the water/oil and water/air interfaces.[30−34] Prior work showed that H_2 and H_2O_2 are spontaneously generated via reduction in SEWMs, and a significant oxidative transformation of hexadecane to hexadecanol was identified via nuclear magnetic resonance (NMR).[23] Previous studies in SEWMs have also pointed toward the transformation of the oil phase.[35−37] These findings lead to two important questions: Can oil/water microdroplet-enabled redox reactions be extended to renewable, plant-derived oils rather than relying on petroleum products such as hexadecane? Can oil transformations be leveraged to produce value-added products sustainably at the water–oil interface?

In this work, we extend the microdroplet redox narrative by transitioning from petroleum-based alkanes to renewable, plant-based oil. We demonstrate that SEWMs produced with ethyl palmitate (EP), a natural palm oil derivative with multiple applications in the chemical and cosmetic industry, can achieve similar redox outcomes, facilitating the catalyst-free generation of H_2O_2 and H_2. Given that palm oil is a major biofeedstock produced at approximately 72 million metric tons annually worldwide, EP represents a readily available platform for sustainable redox systems.[38] Notably, our results demonstrate an anticorrelation between H_2 and H_2O_2 produced in EP SEWMs, a key observation toward establishing how the redox budget within these microdroplets is utilized. Furthermore, we explore a comprehensive "paired redox" pathway that has been largely overlooked in previous microdroplet studies. We propose that EP does not act merely as a passive solvent but functions as a sacrificial redox agent to close the charge balance. Our results show that while H_2O_2 and H_2 are generated through reduction pathways, the oxidative transformation of EP yields useful organic compounds such as alcohols, aldehyde derivatives, and carboxylic acids. Thus, SEWMs offer a potential path forward providing a new framework for understanding how biomass-driven materials can be leveraged in micro-electrochemical reactors to drive the next generation of sustainable chemical synthesis, on-demand production, modularity, and distribution.

EXPERIMENTAL SECTION

Chemicals and Materials

All microdroplet experiments were performed using ultrapure water from a Millipore Sigma Synergy UV Water Purification System. Ethyl palmitate (≥99%), hexadecane, soluble starch powder, soybean oil, sunflower oil, and corn oil were purchased from Sigma-Aldrich. Potassium nitrate (KNO_3, 99%), potassium iodide (KI, 99%), and hydrogen peroxide (H_2O_2, 30% ACS grade) were obtained from Fisher Chemicals. A platinum (Pt) wire (99.9%) with a diameter of 25 μm was obtained from Goodfellow. The platinum wire counter electrode, with a diameter of 0.4 mm, was purchased from Gamry Instruments. The Ag/AgCl reference electrode was purchased from CH Instruments. Disposable glass scintillation vials purchased from VWR (article no. 66022-128) with a capacity of 20 mL were used for ultrasonication. Centrifugation was performed using a Vulcan Clinaspin centrifuge. 5,5-Dimethyl-1-pyrroline-*N*-oxide (DMPO) was purchased from Enzo Life Sciences. The water-in-oil microdroplets were generated using a Bransonic M1800H ultrasonic bath operating at 70 W and a frequency of 40 kHz. A Hamilton 2.5 mL gas-tight syringe was used for headspace gas chromatography (GC) analysis.

Microscopy and Optics

Bright-field imaging of droplets was performed using an inverted epi-fluorescence microscope (IX71, Olympus), equipped with a CMOS camera (Grasshopper 3, FLIR), which captured images using a 1920 × 1200 pixelated array at 30 Hz. A 0.6 numerical aperture (NA) 40× objective lens (Olympus) was used for imaging.

Electrochemical Detection of H_2O_2

A 12.5 μm Pt-ultramicroelectrode (Pt-UME) was used for the detection of H_2O_2. The electrochemical measurements were conducted using a CH Instruments 601E potentiostat in a Faraday cage.

UV–Vis Spectroscopy

The iodometric detection of H_2O_2 was carried out at room temperature using a Shimadzu UV-1280 Spectrophotometer with a quartz cuvette (with a 1 cm path length). To prepare the samples, 200 μL of the aqueous phase extracted from the ultrasonicated emulsions was added to a mixture of 1 mL of 0.1 M HCl, 200 μL of 1 M KI, and 200 μL of 0.5% (w/v) starch solution. The mixture was allowed to stand for 10 min to ensure the complete reaction of H_2O_2. The resulting dark blue solution was then transferred to a quartz cuvette, and absorbance was recorded at a wavelength of ∼580 nm.

GC Analysis

GC analysis was conducted using a Thermo Fisher Scientific Trace 1610 Permanent Gas Analyzer equipped with dual thermal conductivity detectors (TCD) and an auxiliary valve oven. The oven temperature was maintained at 80 °C. Both TCDs were held at 200 °C with a filament temperature of 300 °C. Reference flows were maintained at 1.0 mL/min (He for Aux L-TCD, N_2 for Aux R-TCD). Samples were injected at a volume of 2.5 mL.

Nuclear Magnetic Resonance (NMR) Spectroscopy

All NMR measurements were conducted on a Bruker NEO 600 MHz NMR spectrometer, equipped with a 5 mm BBO prodigy probe. For analysis of products in the distinct phases after forming SEWMs, 600 μL of the aqueous phase was diluted in 60 μL of D_2O, and 250 μL of the oil phase was diluted in 350 μL of $CDCl_3$ in NMR tubes for ^1H and ^{13}C NMR spectra. ^1H NMR spectra for the aqueous phase were acquired with 128 scans, and ^{13}C NMR spectra were acquired with 10,000 scans. The ^1H NMR spectra for the oil phase were acquired with 64 scans, whereas the ^{13}C NMR spectra were acquired with 512 scans. Two-dimensional heteronuclear single quantum coherence spectroscopy (HSQC) and correlation spectroscopy (COSY)

https://doi.org/10.1021/acssuschemeng.6c05673
ACS Sustain. Chem. Eng. 2026, 14, 15850−15862

spectra of the aqueous phase were recorded with 32 and 16 scans, respectively, and additional HSQC and heteronuclear multiple bond correlation (HMBC) spectra were collected in D_2O with 8 and 128 scans, respectively. For quantitative NMR (qNMR), 48.5 mM triphenylphosphate (TPP) in $CDCl_3$ was used as the external calibration compound. To confirm spectral assignments, the aqueous extract was spiked with authentic standards (1 mM each of acetic and formic acid, 0.5 mM each of ethanol and methanol), and spectra were recorded before and after spiking with 128 scans.

Infrared Spectroscopy

Attenuated total reflectance–surface-enhanced infrared absorbance spectroscopy (ATR-SEIRAS) experiments were performed utilizing a PerkinElmer Spectrum 3 FTIR with a liquid nitrogen-cooled MCT detector. The FTIR was fitted with a VeeMax III (PIKE technologies) specular reflection accessory and coupled with a Jackfish electrochemical cell (PIKE Technologies). The specialized internal reflection element (IRUBIS) was used with a 35° angle of incidence.[39] The spectra were collected between 4000 and 700 cm^{-1} at a 4 cm^{-1} resolution using an 8.94 mm J-stop with a scan speed of 1 cm^{-1} s^{-1}. For SEIRAS measurements, the scan accumulation was 256 scans. All electrochemical ATR-SEIRAS experiments used a CHI 1242C potentiostat (CH Instruments, Inc.) with a carbon rod for the counter electrode and an Ag/AgCl reference electrode (3 M KCl) connected via a 0.1 M $NaClO_4$ agar salt bridge. The internal reflection element and working electrode used for all ATR-SEIRAS experiments were a graphene-on-gold substrate reported in prior work.[40] All EC-SEIRAS experiments used the gold-plated IRE as the working electrode, a carbon rod as the counter electrode, and an Ag/AgCl (3 M) as the reference electrode.

Electron Paramagnetic Resonance (EPR) Spectroscopy

5,5-Dimethyl-1-pyrroline-*N*-oxide (DMPO) was utilized as a radical spin trap for the detection of the radical species. For preparing the samples for EPR spectroscopy, a 1:10 water-ethyl palmitate mixture was prepared by adding 200 μL of 50 mM aqueous DMPO to 2 mL of oil in a 20 mL glass scintillation vial and ultrasonicating for 25 min under continuous oxygen purging conditions. The aqueous phase for EPR measurements was then removed after centrifugation of the emulsion formed. Aliquots of the water phase were transferred to a Wilmad Glass quartz flat cell. The spectra were acquired at room temperature (~298 K) with an EMXPlus X-band instrument. The measurements conditions were center field = 3480 G, sweep width = 100 G, sweep time = 30 s, averages = 8 scans, microwave power = 20 mW, receiver gain = 30 dB, modulation amplitude = 1 G, and microwave frequency = 9.783382 GHz.

RESULTS AND DISCUSSION

H_2O_2 Generation from Ethyl Palmitate (EP)-Based Microdroplets

EP-based SEWMs were generated using ultrasonication at a frequency of 40 kHz (Figure 1a). Vials containing different water-to-oil ratios of 10:1, 5:1, 1:5, and 1:10 were ultrasonicated to determine the optimal ratio to identify the water-to-oil ratio that resulted in the highest hydrogen peroxide and hydrogen production among the conditions tested (Note S1 and Figure S1). This resulted in the formation of a homogeneous emulsion. Although we attempted to measure the zeta potential and characterize microdroplet size distribution using dynamic light scattering, our efforts were unsuccessful as the highly

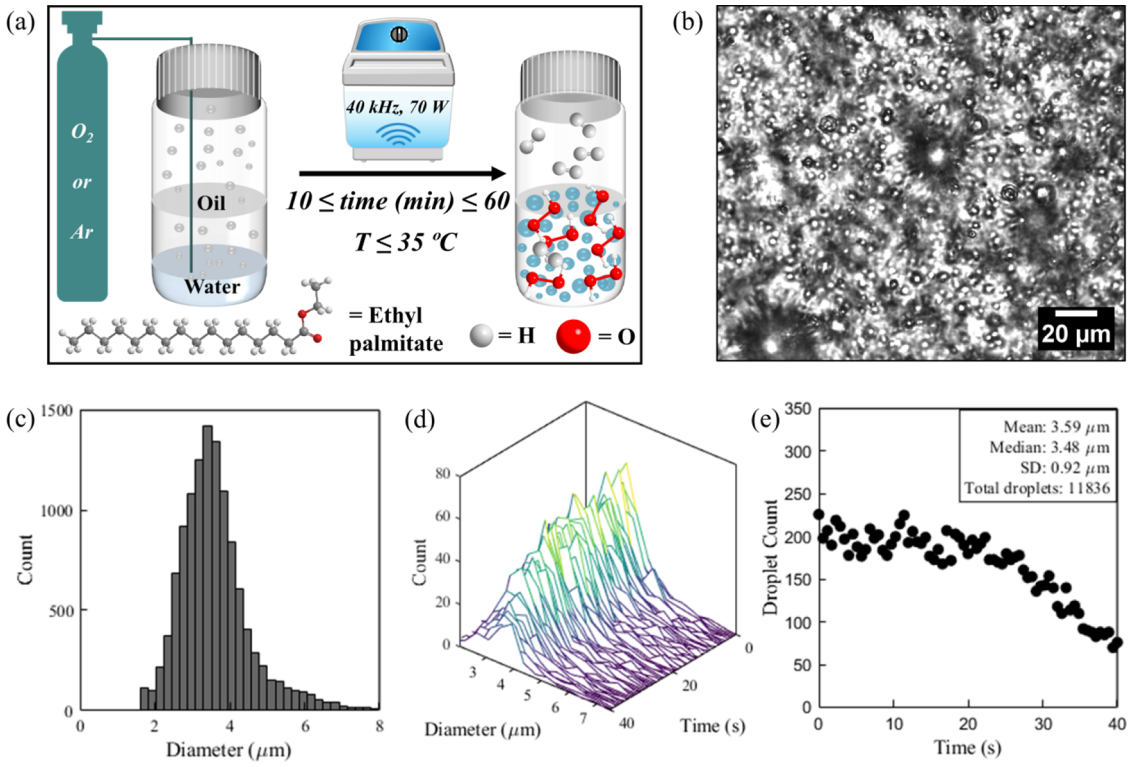

Figure 1. (a) Schematic of the experimental setup. (b) Optical image of microdroplets formed during ultrasonication of a 1:10 ratio of water and ethyl palmitate. (c) Size distribution of microdroplets (diameter in μm) as a function of time during ultrasonication. (d) Distribution of the droplet diameter as a function of time after ultrasonication, with the color intensity and *z*-axis representing the number of droplets detected per frame (not unique individual droplets) in each time-size bin. (e) Distribution of the droplet count over time, where the droplet count represents the number of droplets detected per frame (not unique individual droplets).

https://doi.org/10.1021/acssuschemeng.6c05673
ACS Sustain. Chem. Eng. 2026, 14, 15850−15862

dynamic nature of the formed microdroplets, the lack of surfactant, and the large amounts of oil in some compositions resulting in high turbidity rendered such results unreliable. Consequently, bright-field optical microscopy combined with digital image analysis was used that allowed us to directly observe the microdroplets and obtain a size distribution histogram without the aforementioned physical limitations. Figure 1b shows a characteristic image of 1:10 water-to-EP SEWMs generated under ambient conditions for 5 min of ultrasonication (Note S2). We determined the size distribution of the water microdroplets over a 40 s time after ultrasonication for 5 min (Figure 1c), and the average size of microdroplets generated was 3.5 ± 0.9 μm. Figure 1d shows the temporal analysis of the microdroplets over a glass slide after the samples were sonicated for 5 min and a ∼10 s transfer to the microscope. For at least ∼40 s, the emulsions were sufficiently stable on the glass slide for imaging. The full analysis of these results for the different water-to-EP ratios (Figures S2–S4) shows that the number of droplets and their size changed dramatically when comparing different compositions. In the water-rich compositions (10:1 and 5:1), the droplets consisted of oil rather than water, whereas in the oil-rich compositions (1:5 and 1:10), the droplets consisted of water, i.e., strictly ultrasonicated emulsified water microdroplets (SEWMs). Bright-field microscopy imaging analysis revealed that a 1:10 ratio of water-to-EP generated the largest number of SEWMs obtained across this set of conditions. Notably, temporal changes in the per-frame droplet counts suggest progressive droplet coalescence over time (Figure 1e and Figures S2–S4).

To assess the reactivity of water/EP microdroplets on the spontaneous generation of H_2O_2, we first ultrasonicated the oil/water mixtures under ambient conditions (i.e., in an open system exposed to oxygen from air) for 30 min. The emulsions were then centrifuged to extract the aqueous phase containing H_2O_2. Peroxide formation was detected electrochemically using a Pt-ultramicroelectrode and confirmed using commercial H_2O_2 detection strips via a colorimetric assay using a peroxidase-catalyzed reaction. Although the peroxide strips showed a small amount of H_2O_2 generated in the 10:1 and 5:1 system of ∼30 μM, a larger amount was detected in the 1:5 and 1:10 systems with ∼0.6 and ∼0.8 mM each, implying at least one order of magnitude increase in the concentration. Cyclic voltammograms for H_2O_2 detection, shown in Figure 2a–d, indicated stark differences for samples with an excess of oil (1:10, 1:5) compared to an excess of water (10:1, 5:1), with only the former clearly showing the formation of detectable amounts of H_2O_2. Chronoamperometry measurements performed using a Pt-UME biased at 0.9 V vs an Ag/AgCl/3 M KCl corroborated this result (Figure S5a,b). H_2O_2 concentrations were obtained using a calibration curve (Figure S5c,d), which showed that 1:5 and 1:10 ratios of water-to-ethyl palmitate produce ∼0.8 and ∼1.4 mM H_2O_2, respectively. Overall, these measurements showed an increase in the concentration of H_2O_2 with an increasing amount of oil in the system, conditions under which water-in-oil microdroplets form, i.e., strictly SEWMs.

H_2 Generation from Ethyl Palmitate (EP)-Based Microdroplets

We next characterized hydrogen gas generation from SEWMs in Ar-purged solutions (i.e., in the absence of O_2 from air). Combinations of 10:1, 5:1, 1:5, and 1:10 ratios of water-to-EP

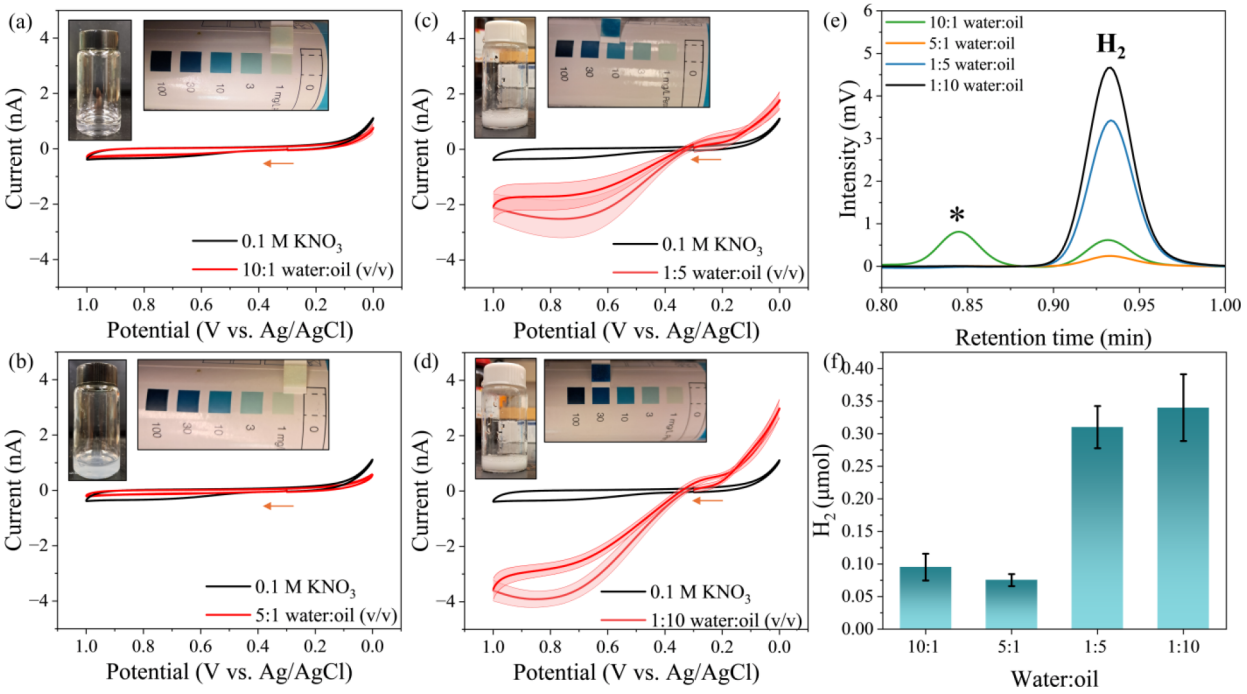

Figure 2. H_2O_2 and H_2 generation as a function of the water:oil ratio. Cyclic voltammograms (CVs) showing H_2O_2 oxidation responses in the water phase from emulsions formed by ultrasonication of (a) 10:1, (b) 5:1, (c) 1:5, and (d) 1:10 water-to-oil ratios. The CVs were recorded in a three-electrode setup using a 12.5 μm Pt-UME. All electrochemical measurements were performed using 0.1 M KNO_3 as the supporting electrolyte, added after extracting the aqueous phase by centrifugation (5× dilution). (e) Gas chromatograms (GC) of samples prepared with varying water:oil ratios after 30 min of ultrasonication under sealed conditions, showing a peak for H_2 detection; the peak labeled * indicates the signal for residual He carrier gas. (f) Corresponding quantified H_2 produced in the headspace of the samples in (e).

https://doi.org/10.1021/acssuschemeng.6c05673
ACS Sustain. Chem. Eng. 2026, 14, 15850−15862

were ultrasonicated under sealed conditions for 30 min to prevent the escape of any gases formed. Gas samples were extracted from the headspace of the sealed vial and analyzed for H_2 using gas chromatography (GC). The amount of H_2 gas evolved was quantified using a calibration curve generated by injecting different volumes of 4.8% H_2 in an Ar gas mixture into the GC, with distinct H_2 peaks at $t \approx 0.94$ min (Figure S6a,b). Gas chromatograms (Figure 2e) and the corresponding amounts of H_2 produced (Figure 2f) quantified using the calibration curve in Figure S6 show once more that the 1:5 and 1:10 ratios of water-to-EP SEWMs generate larger quantities of H_2 compared to the 10:1 and 5:1 ratios of water-to-EP. These results further indicate that water-in-oil microdroplets are more reactive than their oil-in-water counterparts for both H_2O_2 and H_2 generation.

To assess whether the observed H_2O_2 and H_2 were generated specifically due to the formation of the microdroplet interface, we performed control experiments by ultrasonicating pure water and pure oil separately for 30 min under identical conditions. Electrochemical measurements (performed only on ultrasonicated water samples) and peroxide test strips revealed no detectable H_2O_2 in either of these control systems (Figure S7a,b). There was a small measurable signal for H_2 production on pure EP, but results from GC analysis revealed the amount to be 10 times lower compared to the 1:10 water:EP SEWMs (Figure S7c,d). Such quantities are consistent with the amounts observed for the oil-in-water droplets as shown in Figure 2f, suggesting that oil-in-water droplets do not generate H_2 above the background level of pure EP. It is known that ultrasonication can induce H_2 generation in single-phase systems.[41,42]

We further estimated the total interfacial area exposed to the 1:5 vs the 1:10 water-to-EP SEWMs during the initial 40 s postultrasonication window to capture the microdroplets before significant phase separation occurred. Assuming that the imaged droplets within this observation window are representative of the immediate postultrasonication emulsion state, the total surface area was estimated by multiplying the number of analyzed droplets by their average surface area (Note S3). The total surface areas of SEWMs on the microphotographs for the 1:5 and 1:10 water-to-EP ratios were 7.62×10^4 and 4.22×10^5 μm^2, respectively. Our results indicate that the total area exposed in the 1:10 SEWMs is at least one order magnitude larger than in the 1:5 SEWMs, consistent with larger amounts of H_2O_2 generation in the former. While this calculation represents a transient operational estimate rather than a static equilibrium value due to inevitable droplet coalescence over time, this sharp 10-fold increase in the total surface area directly correlates with the larger amounts of H_2O_2 generation observed in the 1:10 system. However, the results for H_2 production are similar in both cases, suggesting that the total area exposed in each case is not the sole driver of differences in reactivity. Prior work has shown that microdroplet reactivity, particularly with respect to H_2O_2 formation, increases with the decreasing droplet radius.[43,44] Consistent with this trend, our experimental results indicate that microdroplets formed at a 1:5 water-to-EP ratio are larger than those formed at a 1:10 ratio (Figure 1e and Figure S4d), providing additional support for the enhanced H_2O_2 formation observed in the latter system. Our results clearly show that the production of two redox products, H_2 and H_2O_2, is significantly increased in SEWMs involving at least 1:5 and 1:10 water:EP in contrast to single phases, highlighting a unique chemical effect that underscores the critical role of the water–oil microdroplet interface. Based on these results, we focused on characterizing the 1:10 water-to-oil ratio SEWMs, which generated significant amounts of H_2O_2 and H_2 for subsequent experiments.

We next turned to enhancing the generation of H_2O_2 and H_2 from the most reactive 1:10 SEWM system using EP under varying ultrasonication times. The corresponding SEWMs were prepared by ultrasonicating the 1:10 water-ethyl palmitate mixture for 10, 20, 30, and 60 min under ambient conditions (for H_2O_2) and Ar-purged, sealed conditions (for H_2). Electrochemical measurements revealed that H_2O_2 production increased progressively with longer ultrasonication times, as shown in Figure 3a–d and Figure S8a. Across this set of conditions, the maximum amount of H_2O_2 was generated in SEWMs formed by ultrasonicating the emulsions for 60 min, reaching up to 2.4 mM (Figure S8b). This trend can be attributed to the continuous reduction of dissolved oxygen to H_2O_2 and its subsequent accumulation during ultrasonication. Because ultrasonication was carried out under ambient conditions, oxygen from the atmosphere continuously diffused into the samples, thereby sustaining and enhancing peroxide formation. This trend was further supported by the positive iodometric assay. In this assay, H_2O_2 oxidizes iodide (I^-) ions to iodine (I_2), which then forms a blue complex with starch. The increasing absorbance at $\lambda \approx 580$ nm observed with longer ultrasonication times confirmed the formation of higher H_2O_2 concentrations, up to 3.8 mM, as shown in Figure S9. Further, gas chromatograms for H_2 detection also revealed an increase in H_2 production with the increase in ultrasonication time (Figure 3e,f). This trend arises from the sustained formation of reactive microdroplets during ultrasonication, which continuously drive redox reactions and allow H_2 to accumulate in the headspace.

Given that ethyl palmitate has an ester functional group, we examined whether this might quench or decompose the generated H_2O_2. To test this, samples containing 10 mM H_2O_2 were ultrasonicated with ethyl palmitate in a 1:10 ratio under Ar for 30 min. The resulting peroxide concentrations were then compared to those from parallel experiments in which water and oil were ultrasonicated under identical conditions without added H_2O_2. As shown in Figure S10, the electrochemical analyses revealed no significant loss of H_2O_2, confirming the chemical stability of H_2O_2 in this system. This was also confirmed statistically using the Welch's *t*-test, which indicated no difference between the expected and experimental concentrations of H_2O_2 (Note S9 and Table S1).

The Redox Budget for H_2 and H_2O_2 Generation

Beyond increasing the yield of H_2 or H_2O_2 by increasing the ultrasonication time, we further sought to understand how the production of these two species is correlated. Here, we modified the atmosphere in which H_2O_2 was produced by forming the emulsions under saturated oxygen conditions while ultrasonicating for 60 min. Increasing dissolved O_2 availability led to substantially higher anodic (oxidative) currents (Figure S11a–c). These results indicate that greater dissolved O_2 availability significantly enhances H_2O_2 generation.[23] Quantitative electrochemical analysis revealed that H_2O_2 concentrations reached up to 8.5 mM after optimal ultrasonication conditions, i.e., ultrasonicating a 1:10 mixture of water and ethyl palmitate under continuous O_2 purging for 60 min (Figure S11d). These results were corroborated by

https://doi.org/10.1021/acssuschemeng.6c05673
ACS Sustain. Chem. Eng. 2026, 14, 15850–15862

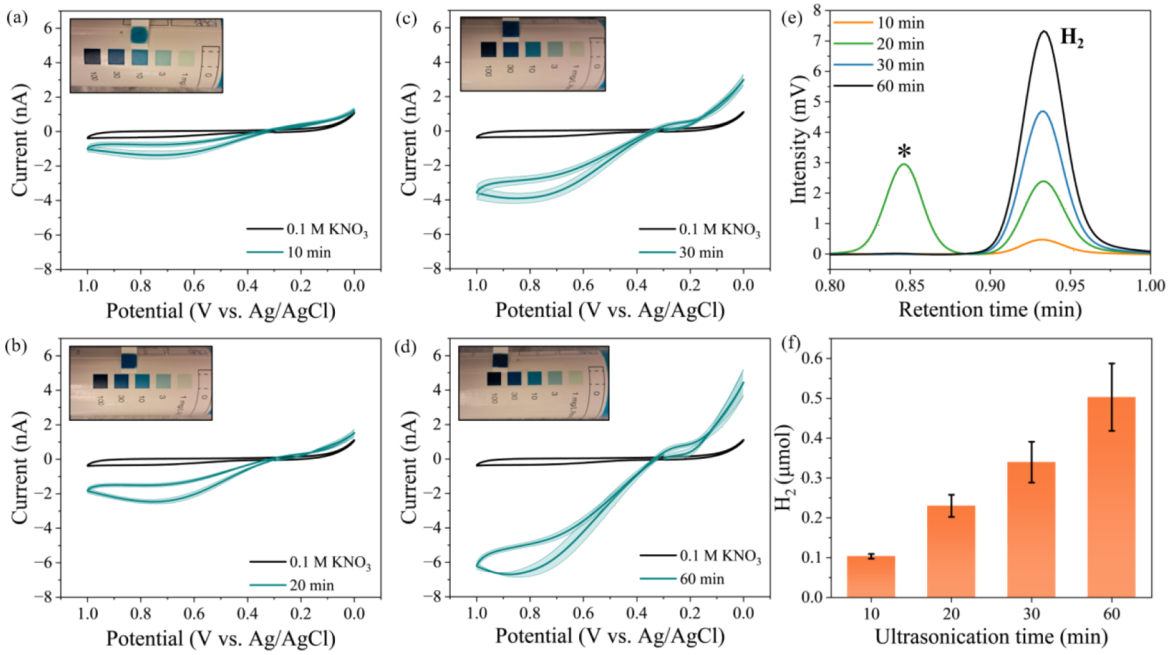

Figure 3. H_2O_2 and H_2 generation as a function of ultrasonication time. Cyclic voltammograms (CVs) showing H_2O_2 oxidation responses in the water phase from emulsions formed by ultrasonication of a mixture of a 1:10 water-to-oil ratio for (a) 10, (b) 20, (c) 30, and (d) 60 min. The increasing current response with increasing ultrasonication time indicates enhanced generation of H_2O_2, corroborated by a corresponding increase in color intensity observed in qualitative peroxide test strips. All measurements were performed after a 5× dilution. (e) Gas chromatograms (GC) of samples prepared with varying ultrasonication times for a 1:10 water:oil sample under sealed conditions; the peak labeled * indicates the signal for residual He carrier gas. (f) Corresponding quantified H_2 produced in the same samples.

complementary UV–vis spectroscopic H_2O_2 detection and quantification (Figure S12a,b) using the iodometric assay. This resulted in 11.3 mM H_2O_2 calculated using the calibration curve (Figure S12c,d) showing good agreement with electrochemical data, indicating method consistency and robustness. Repeated measurements ($n = 3$) demonstrated high reproducibility, with relative standard deviations under 3%.

Although measuring the H_2 generated during continuous oxygenation is not practical due to the open system used in the experiments described above, it is possible to measure H_2 production in an O_2-saturated solution vs that equilibrated with ambient conditions. As shown in the chromatogram in Figure 4a, the SEWMs under an O_2 atmosphere produced significantly lower levels of H_2 compared to those ultrasonicated under ambient air or Ar-purged (oxygen-free) conditions. Both the production of H_2 and H_2O_2 results from reductive processes uniquely triggered in SEWMs, as suggested previously for hexadecane.[23] In oxygen-rich environments, this reducing power is directed toward transforming oxygen to H_2O_2 as the concentration of oxygen rises from ∼0.3 mM in water under ambient conditions to ∼1.1 mM under oxygenation.[45,46] In contrast, under a deoxygenated solution obtained by saturating in argon, the reduction is shifted toward H_2 production. These observations are summarized in Figure 4a and Figure S13a, which highlights an anticorrelated relationship between H_2O_2 and H_2 production, as well as their dependence on the ultrasonication atmosphere. This trend is not specific to ethyl palmitate but is generally observed in microdroplets formed by ultrasonicating water with organic oils such as hexadecane, which was also characterized at a 1:10 ratio under the identical conditions (Figure 4b and Figure S13b). Although hexadecane, a previously studied organic oil in the literature, produces roughly twice the amount of H_2 and H_2O_2 compared to ethyl palmitate, the latter emerges as an attractive alternative utilizing a renewable, biodegradable feedstock, representing a more viable path for decentralized chemical production. This advantage is evident in the discussion below, where we describe the sacrificial role of the oil to produce small organic molecules as a result of closing the redox cycle.

Oxidative Transformation of Ethyl Palmitate at the SEWM Interface

It is a well-established fact that redox processes must be charge-balanced, i.e., the reductive process resulting in the formation of H_2O_2 or H_2 must be accompanied by an oxidation. Here, we characterize the ability of SEWMs to induce the oxidation of EP during ultrasonication. We performed NMR measurements on the aqueous phase obtained after ultrasonicating an 1:10 water:EP mixture for an hour under continuous O_2 purging. Results from ^{1}H NMR analysis showed the appearance of numerous new signals upon ultrasonication. Upon structural analysis based on the chemical shift values, integrations, and the splitting pattern of each NMR peak, we identified a triplet at 1.08 ppm and a corresponding quartet at 3.56 ppm corresponding to ethanol, a singlet at 1.96 ppm corresponding to acetic acid, a singlet at 3.27 ppm corresponding to methanol, and a singlet at 8.3 ppm corresponding to formic acid (Figure 5a). These assignments were corroborated by ^{13}C NMR (Figure 5b), which showed characteristic signals for each compound, and further confirmed through 2D-^{1}H-^{13}C HSQC and 2D-^{1}H-^{1}H COSY spectra (Figures S14 and S15). Additional verification was achieved by spiking the sample with

https://doi.org/10.1021/acssuschemeng.6c05673
ACS Sustain. Chem. Eng. 2026, 14, 15850−15862

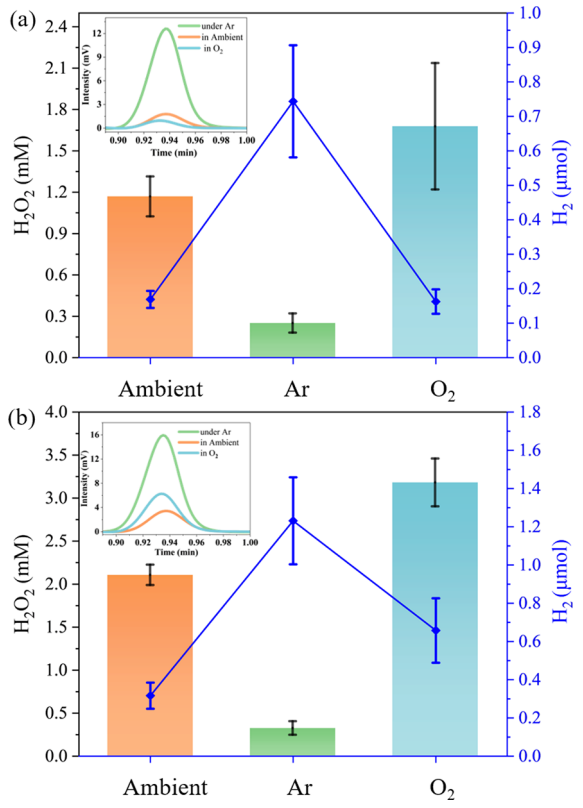

Figure 4. Correlation plots illustrating an inverse relationship between the amount of H_2O_2 and H_2 produced under ambient, Ar-, and O_2-saturated conditions for (a) ethyl palmitate and (b) hexadecane. Gas samples were extracted from the headspace of sealed vials, and 2.5 mL was injected into the GC using He as the carrier gas. H_2O_2 concentrations were determined electrochemically from the aqueous phase of the same samples.

known standards of each compound, which increased the corresponding peak intensities (Figure S16 and Table S2).

Two intense additional resonances at 81.72 and 92.66 ppm in the ^{13}C NMR were observed (Figure 5b). These peaks did not show clear cross-correlation peaks in the 2D-HSQC due to overlap with a strong residual water signal (Figure S14). To identify these peaks, the experiment was repeated using D_2O instead of H_2O under the identical conditions. Under these conditions, correlations were observed at 4.74 ppm/81.72 ppm and 4.96 ppm/92.66 ppm in the $^1H/^{13}C$ spectra, respectively (Figure 5c). Additionally, both cross peaks displayed the opposite phase relative to the CH/CH_3 signals in this multiplicity-edited HSQC (Figure S17), indicating that they correspond to a CH_2 group bonded to an electronegative substituent. The signal pair at 4.74 ppm/81.72 ppm is assigned to methanediol, with a structure shown in Figure 5c and supported by HMBC analysis (Figure S18). The latter analysis only showed the doublet centered at 4.74 ppm with a ^1J-CH coupling constant of ~163.4 Hz, consistent with a CH_2 group directly bonded to a carbon bearing two electronegative substituents, and a downfield ^1H shift also corroborated hydroxyl substitution. We further confirmed this species through the agreement with the ^1H and ^{13}C spectra of the methanediol standard measured in water/D_2O (Figure S19). We provide additional evidence for the presence of methanediol through SEIRAS measurements, which showed a characteristic band at ~1030 cm^{-1} (Figure S20a).[47] Potential-dependent SEIRAS further confirmed its identity: the signal diminished under oxidizing potentials, consistent with conversion of methanediol to formic acid (Figure S20b). The second correlation at 4.96 ppm/92.66 ppm arose from a species that was also formed reproducibly under these conditions. Based on its chemical shifts, the absence of observable proton–proton coupling (singlet), and the concurrent formation of short-chain alcohols and acids, we tentatively attributed this resonance to oxydimethanol. The observed ^1H and ^{13}C chemical shifts closely matched those predicted from simulated spectra (Figure S21).

Quantification of the identified peaks was carried out by qNMR using triphenylphosphate (TPP, 48.5 mM in $CDCl_3$) as an external calibration standard. The calculated concentrations of methanol, ethanol, formic acid, and acetic acid are 0.44, 0.79, 4.10, and 2.93 mM, respectively. The concentrations of methanediol and oxydimethanol were determined from the ^{13}C spectrum by comparing their integrals to that of the methylene carbon of ethanol. Although ethanol generally has the longest T1 (spin-lattice relaxation) among the three compounds, under the current ^{13}C acquisition parameters, its signal intensity is likely lower than that of a fully relaxed spectrum. As a result, using the ^{13}C intensity of ethanol as a reference may overestimate the concentrations of the other two compounds. Nevertheless, the integration ratio of ethanol:methanediol:oxydimethanol is 1:7.24:6.17, resulting in estimated concentrations for methanediol of 5.72 and 2.44 mM for oxydimethanol. These results are summarized in Table S3.

No new peaks were detected in the oil phase, suggesting that only small, water-soluble products were formed (Figure 5d and Figure S22). Together, these findings demonstrated that SEWMs formed under saturated oxygen conditions (most reactive) produced ethanol and oxidative products (formic and acetic acid, methanol, methanediol, and oxydimethanol). This mixture of oxidized C_1–C_2 compounds highlights the dual redox nature of microdroplet environments, where ROS formation (notably via two-electron reduction of O_2 to H_2O_2) occurs simultaneously with oxidative fragmentation of the organic phase. Moreover, a balance is observed between reduction products (H_2O_2 and H_2) and oxidation products, as detailed in the following section. This redox behavior underscores the potential of SEWMs as self-sustaining reaction environments capable of driving spontaneous chemical conversions without added catalysts.

Mechanistic and Redox Analysis

We posit that a balance sheet of redox equivalents reflecting the charge exchange across the oil–water microdroplet interface is useful to understand the mechanistic pathways for paired redox in SEWMs generated by EP. This is because the oxidation of ethyl palmitate fragments should be counterbalanced by reductive processes, which we primarily ascribe to the two-electron ORR of dissolved oxygen at the microdroplet interface:[23]

$$O_2 + 2H^+ + 2e^- \rightarrow H_2O_2$$

The continuous generation and subsequent redox or thermal homolysis of H_2O_2 create conditions for hydroxyl radical (·OH) generation in SEWMs.[23] Furthermore, we posit that H_2 generation is an additional plausible electron sink. As

https://doi.org/10.1021/acssuschemeng.6c05673
ACS Sustain. Chem. Eng. 2026, 14, 15850–15862

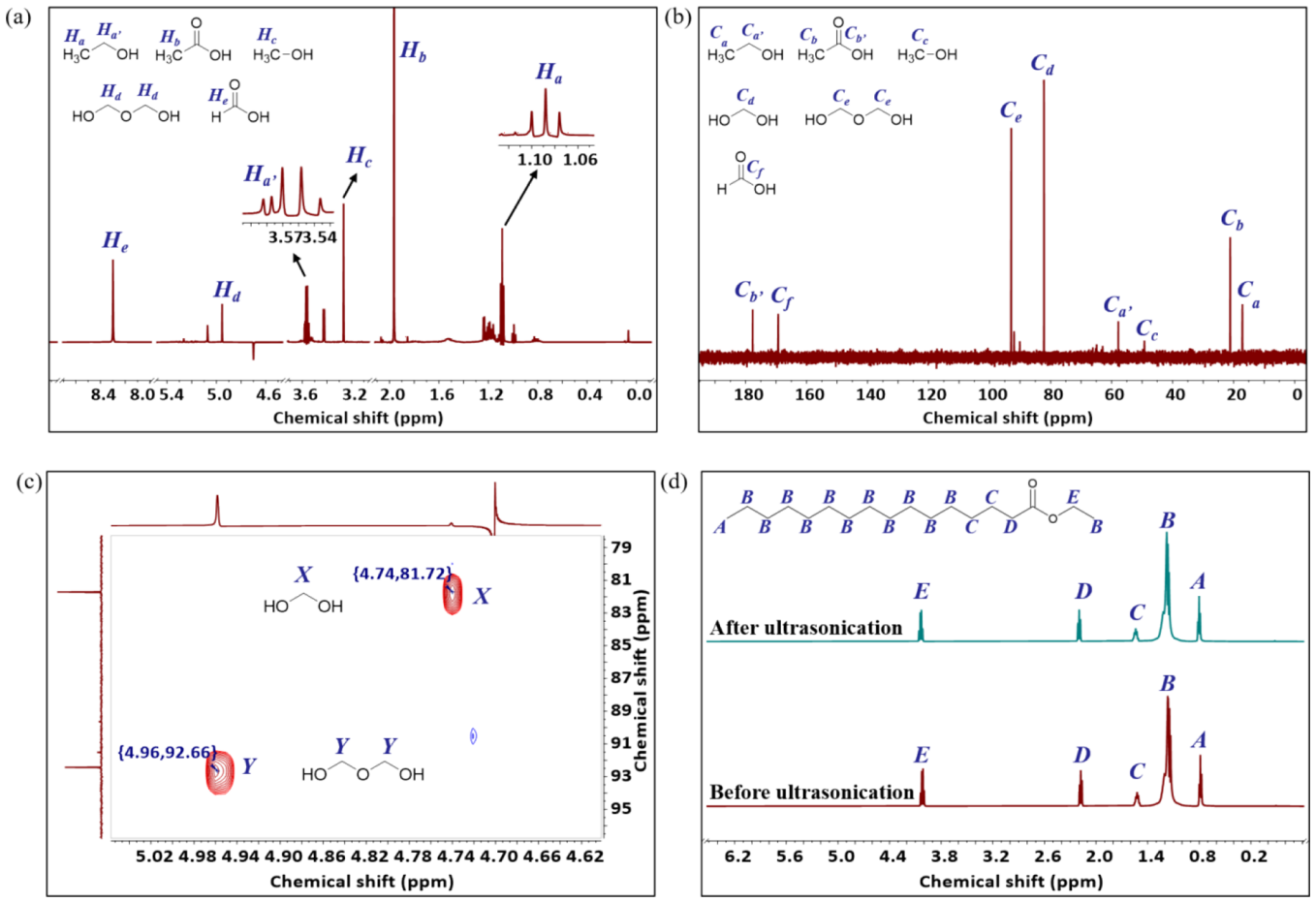

Figure 5. Formation of small water-soluble molecules via oxidative transformation of ethyl palmitate during microdroplet generation. (a) ^{1}H NMR (600 MHz, H_2O/D_2O): δ 1.08 (t, J = 7.22 Hz, 3H, H_a), 1.96 (s, 3H, H_b), 3.27 (s, 3H, H_c), 3.56 (q, J = 7.18 Hz, 2H, $H_{a'}$), 4.95 (s, 4H, H_d), 8.3 (s, 1H, H_e); the negative peak represents water suppression signal. We do not observe the signal for methanediol in ^{1}H NMR as it is suppressed during water suppression. Signals for hydroxyl protons were also not observed as these protons undergo rapid exchange with water. (b) ^{13}C NMR (151 MHz, H_2O/D_2O): δ 17.11 (C_a), 21.1 (C_b), 49.25 (C_c), 57.79 ($C_{a'}$), 81.72 (C_d), 92.66 (C_e), 169.29 (C_f), 177.67 ($C_{b'}$) of the aqueous phase extracted from the emulsion generated by ultrasonicating a 1:10 ratio of water and ethyl palmitate under a saturated oxygen environment. (c) HSQC 2D NMR of the aqueous phase extracted after an hour of ultrasonication of a 1:10 ratio of D_2O-to-ethyl palmitate under saturated O_2 conditions, for structural correlation and assignments of the NMR peaks obtained for methanediol and oxydimethanol. The NMR spectrum was acquired in D_2O. The red contours represent the presence of CH_2 groups. The peak with a negative and positive signal at 4.7 ppm represents the water suppression signal. (d) ^{1}H NMR (600 MHz, $CDCl_3$): δ 0.79 (t, 3H, A), 1.13–1.25 (m, 25H, B), 1.52 (m, 4H, C), 2.18 (t, 2H, D), 4.02 (q, 2H, E) of ethyl palmitate before and after ultrasonication; it shows no visible difference in the oil phase before and after ultrasonic treatment.

demonstrated by Chen and co-workers, interfacial electric fields at the biphasic oil–water boundary can drive the formation of H_2 from water.[35] Asserghine and co-workers reported that SEWMs generate sufficient reducing driving force for H_2 evolution either via combination of ·H generated from oil degradation or via the hydrogen evolution reaction involving protons in the aqueous solution.[23] Together, these complementary reductive sinks effectively balance the concurrent oxidation of the oil phase. Regarding this oxidation, two pathways have been described in the sonochemical literature to account for the degradation of organic compounds: (1) pyrolytic thermal reactions induced by bubble cavitation, which occurs especially in solvents of high volatility, and (2) formation of high energy radicals, e.g., ·OH, and subsequent reaction with the surrounding media.[42,48,49] In particular for long chain nonvolatile alkanes, C–C bond cleavage leads to the formation of alkyl radicals through sonochemical effects (e.g., ethyl and methyl).[42] Additionally, it has been reported by Chen and co-workers that oils such as hexadecane undergo oxidative cracking in the presence of microdroplet-generated ROS such as ·OH.[35] These alkyl radicals together with the microdroplet-mediated formation of ·OH create conditions to form species such as methanol and ethanol. We hypothesize that the subsequent oxidation of these alcohols leads to the formation of methanediol (hydrated form of formaldehyde), oxydimethanol (condensation product of formaldehyde and methanediol), acetic acid, and formic acid. One of the defining features of SEWMs is that, distinct to ultrasonication of a single-phase system, the biphasic system helps accelerate reactivity and increase the yield of redox products (i.e., H_2O_2 as we previously reported).[23] To this point, one of the levers that we can use to explore product formation is regulating the source of redox, in this case, controlling the

https://doi.org/10.1021/acssuschemeng.6c05673
ACS Sustain. Chem. Eng. 2026, 14, 15850–15862

oxygenation of the emulsion. To show radical formation in SEWMs, we performed EPR on a 1:10 ratio of water-to-ethyl palmitate sample containing 50 mM DMPO as the radical trapping agent, under continuous oxygen conditions. We observed a strong signal for the DMPO-OH adduct, indicating the formation of highly oxidizing ·OH, which could further generate oxygenated products by reacting with the EP (Figure S23).

Another way of exploring the impact of ROS such as ·OH is to compare product distribution in the presence and absence of O_2. We generated microdroplets by ultrasonicating a 1:10 ratio of water and ethyl palmitate in an Ar environment for 60 min. The sample was purged with Ar for 20 min and then properly sealed to ensure that no oxygen could diffuse into the system. After 60 min of ultrasonication, the emulsion was centrifuged and the aqueous phase was characterized using ^{1}H NMR. We observed the formation of methanol, ethanol, formic acid, and acetic acid (Figure S24a). However, the concentration of organic products obtained in this sample is significantly lower than in samples purged with oxygen (Table S4). For example, formic acid production decreased 35-fold in the absence of oxygen, showing the necessity of this coreactant to perform subsequent oxidation of alcohols to form aldehydes and acids in significant amounts. Critically, we did not observe the formation of methanediol and oxydimethanol in an Ar-purged sample. Sonolysis in (single-phase) solutions saturated with Ar, compared to those saturated with O_2, has been shown to improve the degradation of organic compounds due to differences in the cavitation efficiency.[48] If previously described sonochemical effects were uniquely responsible for the effects observed here, we would expect an increase in the yield of organic compounds in Ar-saturated SEWMs instead of a decrease. Lastly, we ultrasonicated pure ethyl palmitate under continuous O_2 purging conditions for 60 min, followed by ultrapure water wash three times to extract any small organic products formed. ^{1}H NMR shows that there is a formation of the above-mentioned products (Figure S24b), but their concentration is ∼1.5 orders of magnitude less than the reported concentrations for the biphasic system (Table S4). These results reveal an interaction leading to redox processes between water and oil that is unique to SEWMs.

To better understand the electron sources and sinks of redox species, we analyzed the redox equivalents for species formed within a formal redox framework. To construct the overall electron balance, oxidation products and H_2O_2 concentrations were evaluated under continuous O_2 purging for 60 min. Since continuous gas flow prevents the collection of gaseous products formed, H_2 evolution was determined using a sealed setup for 60 min, which allows for headspace gas accumulation, providing a representative quantification of H_2. In this analysis, the formation of H_2O_2 via the 2-electron ORR and H_2 formation via proton reduction represent the identified electron sinks, while the formation of organic products (methanol, ethanol, methanediol, oxydimethanol, formic acid, and acetic acid) through the oxidation of ethyl palmitate represents the electron source. This analysis is intended to provide a conceptual accounting of electron flow rather than a definitive, closed reaction mechanism. After mapping the electron source and sinks quantitatively (Tables S5 and S6), we estimated about ∼75 mmol vs ∼22 mmol redox equivalents for oxidation and reduction, respectively, accounting for ∼30% charge balance. This indicates that while H_2O_2 and H_2 are important, identifiable reduction products, they are not the sole electron sinks. Given that oxygen is continuously purged throughout, the remaining ∼70% of the generated electron equivalents could be consumed by the 4-electron reduction of O_2 to water or other unidentified reduction pathways. Additionally, H_2 was quantified via headspace gas extraction, this value strictly represents the gas-phase fraction. Due to gas–liquid equilibrium, a portion of the generated H_2 remains dissolved in the biphasic oil–water emulsion and is therefore unquantifiable by the headspace analysis. In addition, the formation of gaseous products such as CO_2, CO, CH_4, C_2H_2, C_2H_4, and C_2H_6 has been reported previously in microdroplets generated by ultrasonication of hexadecane and water.[35] Although not quantified in the primary electron balance, the generation of these volatile species could serve as an additional pathway for redox transformation of ethyl palmitate. Furthermore, the shift in reaction environments for H_2 evolution likely alters the product distribution, adding to the greater difference in our calculations for redox balance. Finally, as we have mentioned before while discussing the origin of ·OH in EP-based SEWMs, it is possible that ·OH derived from H_2O_2 as a reductive product could find its way as an oxidizing agent that would be hard to account for in the amounts reported in Tables S5 and S6. Because of these limitations, a 100% closed quantitative balance was not feasible. Overall, the proposed mechanistic pathways and the approximate electron-equivalent balance confirm that despite the complexity of the system, oxidative transformation of oil is coupled to a degree to the generation of reduction products and is summarized in Figure 6.

Exploring Other Plant-Based Oils

To explore the broader applicability of microdroplet formation beyond hexadecane and ethyl palmitate, we extended our study to include various common vegetable oils such as soybean oil, corn oil, and sunflower oil. Detailed characterization and yield comparisons for these systems are provided in the Supporting Information (Supplementary Note S14 and Figures S25 and S26). Furthermore, we have compared the yields of the two reduction products, H_2O_2 and H_2, among various oils tested so far in this work against hexadecane (Figure S27). The consistent generation of H_2O_2 and H_2 across all the tested oils strongly verifies the universality of the system, opening new opportunities to tune microdroplet reactivity using other oils, thereby enabling broader applications and control in renewable chemistry.

■ CONCLUSIONS

In this work, we established that sonicated emulsive aqueous microdroplet formation and their chemistry are not limited to petroleum oils, such as hexadecane; a variety of bioderived, renewable oils such as ethyl palmitate can also serve as alternatives. We found that a 1:10 water-to-ethyl palmitate ratio yields SEWMs producing the maximum H_2O_2 and H_2. H_2O_2 generation was enhanced by continuously purging with O_2 during ultrasonication, whereas O_2-free conditions boost H_2 generation and decrease the formation of H_2O_2, suggesting that these reduced products are the result of a budgeted, redox-mediated process at the oil/water interface.

Critically, our results identified a redox balance where the EP oil phase underwent catalyst-free oxidative transformation into various small, organic molecules such as methanol, ethanol, acetic acid, formic acid, methanediol, and oxydimethanol during

https://doi.org/10.1021/acssuschemeng.6c05673
ACS Sustain. Chem. Eng. 2026, 14, 15850−15862

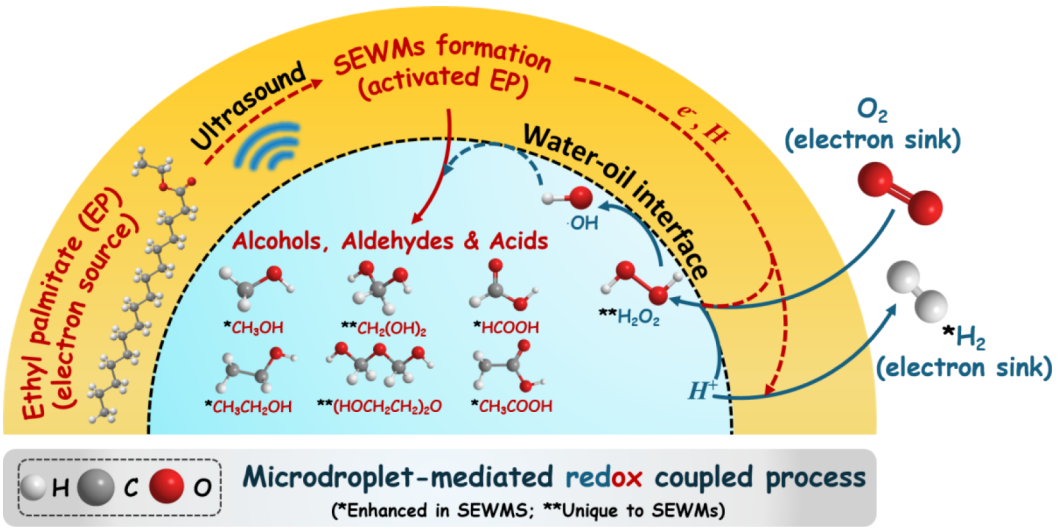

Figure 6. Proposed catalyst-free mechanistic redox reaction pathways occurring at the water–oil interface in ultrasonicated emulsive water microdroplets (SEWMs) generated using plant-based ethyl palmitate. Ethyl palmitate acts as the electron source as it is oxidized to various organic oxidation products such as methanol, ethanol, methanediol, oxydimethanol, formic acid, and acetic acid. This oxidation of the oil is primarily coupled to the reduction of oxygen to form H_2O_2 and reduction of protons or radical combination of ·H to form H_2 gas. Products marked with * exhibit enhanced concentrations in SEWMs compared with sonochemical degradation of the single-phase pure components, whereas products marked with ** are unique to SEWMs and are not detected during sonochemical degradation. Red indicates oxidation pathways, and blue indicates reduction pathways.

the reductive formation of H_2O_2. The formation of these products resquires some degree of redox activation and C–H and C−C cleavage, which are uniquely provided by these catalyst-free microdroplets. Moreover, we found that the formation of SEWMs and, consequently, their reactivity are influenced by the chemical composition and viscosity of the oil used.

The interfacial reactivity for SEWMs described here could support multielectron processes with implications ranging from atmospheric chemistry to sustainable chemical synthesis.[50] One potential application would be the on-demand production of species like H_2, thus turning the oil into a hydrogen carrier, or the in situ generation of species like H_2O_2, which in combination with different oil chemistries under ultrasonication could be leveraged to drive the selectivity of these reactions. From a practical perspective, the steady-state concentrations of H_2O_2 (8.5–11.3 mM; ∼0.03 wt %) in our system are below those of bulk industrial commodities (30–50 wt %). Consequently, the primary utility of the SEWM platform may not lie in centralized, energy-intensive chemical isolation, but rather in decentralized, in situ utilization. Millimolar thresholds of H_2O_2 coupled with active ·OH generation can be directly used in situ for downstream oxidation, disinfection, or environmental remediation applications.[51] While SEWMs offer a powerful, catalyst-free platform for sustainable synthesis, practical deployment requires addressing the inherent limitations of sonochemical scaleup.[52] The conventional batch scaleup is inefficient due to the localized nature of acoustic cavitation and nonuniform energy distribution.[53] Instead, moving toward continuous-flow sonochemical reactors with minimized path lengths represents the most viable path to ensure uniform acoustic energy distribution.[54] Overall, the catalyst-free nature of these systems, and their instrumental simplicity, with reactions carried out in low-cost ultrasonic baths, makes them greatly attractive to explore applications of these sonochemically triggered redox processes for sustainable chemical production from biofeedstocks such as plant-based oils.

■ ASSOCIATED CONTENT

Data Availability Statement

The data supporting this article have been included as part of the Supporting Information (SI). The original raw datasets are also available within the Supporting Information as source data files.

Supporting Information

The Supporting Information is available free of charge at https://pubs.acs.org/doi/10.1021/acssuschemeng.6c05673.

Experimental details; photographs of the experimental setup; bright-field microscopy imaging analyses of emulsions formed by water/oil (ethyl palmitate, soybean oil, corn oil, and sunflower oil); calibration curves for H_2O_2 and H_2; mathematical framework for interfacial area calculation; cyclic voltammograms, chronoamperograms, absorbance spectra, and infrared and SEIRAS spectra of the aqueous phase obtained after centrifugation of the ultrasonicated emulsions; photographs of peroxide strips showing H_2O_2 formation; photographs of the aqueous phase of the ultrasonicated samples after the iodometric assay; gas chromatograms for H_2 detection; ^1H, ^{13}C, HSQC, COSY, and HMBC spectra of the aqueous phase obtained after centrifugation of the ultrasonicated emulsions; ^{13}C NMR of ethyl palmitate; simulated ^1H and ^{13}C NMR of oxydimethanol; EPR spectra of the aqueous phase obtained after centrifugation of the 1:10 water:ethyl palmitate emulsion; bar plots quantifying H_2O_2 and H_2; tables quantifying organic products under different ultrasonication environments;

https://doi.org/10.1021/acssuschemeng.6c05673
ACS Sustain. Chem. Eng. 2026, 14, 15850−15862

table showing electron equivalents of identified oxidation and reduction products; and references (PDF)

Raw data files (ZIP)

AUTHOR INFORMATION

Corresponding Author

Joaquín Rodríguez-López – *Department of Chemistry, University of Illinois Urbana-Champaign, Urbana, Illinois 61801, United States; Beckman Institute for Advanced Science and Technology, University of Illinois Urbana-Champaign, Urbana, Illinois 61801, United States;* orcid.org/0000-0003-4346-4668; Email: joaquinr@illinois.edu

Authors

Sonam Rani – *Department of Chemistry, University of Illinois Urbana-Champaign, Urbana, Illinois 61801, United States; Beckman Institute for Advanced Science and Technology, University of Illinois Urbana-Champaign, Urbana, Illinois 61801, United States;* orcid.org/0009-0000-7767-4239

Hung V. Nguyen – *Beckman Institute for Advanced Science and Technology, University of Illinois Urbana-Champaign, Urbana, Illinois 61801, United States; Department of Materials and Science Engineering, University of Illinois Urbana-Champaign, Urbana, Illinois 61801, United States*

Lingyang Zhu – *School of Chemical Sciences NMR Laboratory, University of Illinois Urbana-Champaign, Urbana, Illinois 61801, United States;* orcid.org/0000-0002-6657-271X

Supriya Das – *Department of Chemistry, University of Illinois Urbana-Champaign, Urbana, Illinois 61801, United States; Beckman Institute for Advanced Science and Technology, University of Illinois Urbana-Champaign, Urbana, Illinois 61801, United States*

Charles M. Schroeder – *Beckman Institute for Advanced Science and Technology, University of Illinois Urbana-Champaign, Urbana, Illinois 61801, United States; Department of Materials and Science Engineering, University of Illinois Urbana-Champaign, Urbana, Illinois 61801, United States*; Present Address: Department of Chemical and Biological Engineering, Princeton University, Princeton, New Jersey 08544, United States; orcid.org/0000-0001-6023-2274

Complete contact information is available at: https://pubs.acs.org/doi/10.1021/acssuschemeng.6c05673

Author Contributions

S.R. and J.R.-L. conceptualized the ideas and supervised the investigations. J.R.-L. acquired the funding. S.R. performed the core experiments, visualized the data, and analyzed the results. S.R. and H.V.N. performed the microdroplet imaging experiments. H.V.N. and C.MS. developed the methodology for microdroplet imaging and performed their visualization and analysis. S.D. assisted in acquiring the SEIRAS data, and L.Z. assisted in the analysis of the NMR data. S.R. and J.R.-L. wrote the manuscript and the Supporting Information. All authors participated in the discussion and helped in reviewing and editing the final manuscript.

Notes

The authors declare no competing financial interest.

ACKNOWLEDGMENTS

This material is based upon work supported by the U.S. Department of Energy, Office of Science, Science Foundations for Energy Earthshots Program, under Award Number DE-SC0024892. Disclaimer: "This report was prepared as an account of work sponsored by an agency of the United States Government. Neither the United States Government nor any agency thereof, nor any of their employees, makes any warranty, express or implied, or assumes any legal liability or responsibility for the accuracy, completeness, or usefulness of any information, apparatus, product, or process disclosed, or represents that its use would not infringe privately owned rights. Reference herein to any specific commercial product, process, or service by trade name, trademark, manufacturer, or otherwise does not necessarily constitute or imply its endorsement, recommendation, or favoring by the United States Government or any agency thereof. The views and opinions of authors expressed herein do not necessarily state or reflect those of the United States Government or any agency thereof." The authors also acknowledge the UIUC School of Chemical Sciences Electron Paramagnetic Resonance Laboratory and Aditi Prasad for assistance.

REFERENCES

(1) Xia, R.; Overa, S.; Jiao, F. Emerging Electrochemical Processes to Decarbonize the Chemical Industry. *JACS Au* **2022**, *2* (5), 1054–1070.

(2) Levin, T.; Bistline, J.; Sioshansi, R.; Cole, W. J.; Kwon, J.; Burger, S. P.; Crabtree, G. W.; Jenkins, J. D.; O'Neil, R.; Korpås, M.; Wogrin, S.; Hobbs, B. F.; Rosner, R.; Srinivasan, V.; Botterud, A. Energy Storage Solutions to Decarbonize Electricity through Enhanced Capacity Expansion Modelling. *Nat. Energy* **2023**, *8* (11), 1199–1208.

(3) Hu, B.; Cheng, A.; Li, Y.; Huang, Y.; Liu, J.; Zhang, B.; Li, K.; Zhao, L.; Wang, T.; Lu, Q. A Sustainable Strategy for the Production of 1,4:3,6-Dianhydro-α-d-Glucopyranose through Oxalic Acid-Assisted Fast Pyrolysis of Cellulose. *Chem. Eng. J.* **2022**, *436*, No. 135200.

(4) Malehmirchegini, L.; Chapman, A. J. Strategies for Achieving Carbon Neutrality within the Chemical Industry. *Renewable Sustainable Energy Rev.* **2025**, *217*, No. 115762.

(5) *Chemicals Value Chain Decarbonization: Integrated Solutions for a Complex Challenge*. Energy.gov. https://www.energy.gov/cmei/ito/articles/chemicals-value-chain-decarbonization-integrated-solutions-complex-challenge (accessed 2026-05-15).

(6) Campos-Martin, J. M.; Blanco-Brieva, G.; Fierro, J. L. G. Hydrogen Peroxide Synthesis: An Outlook beyond the Anthraquinone Process. *Angew. Chem., Int. Ed.* **2006**, *45* (42), 6962–6984.

(7) Ruan, Q. Towards Sustainable H_2O_2 Photogeneration: Advancements, Challenges, and Future Prospects. *ChemCatChem* **2023**, *16* (2), No. e202301082.

(8) Qureshi, F.; Yusuf, M.; Arham Khan, M.; Ibrahim, H.; Ekeoma, B. C.; Kamyab, H.; Rahman, M. M.; Nadda, A. K.; Chelliapan, S. A State-of-The-Art Review on the Latest Trends in Hydrogen Production, Storage, and Transportation Techniques. *Fuel* **2023**, *340*, No. 127574.

(9) SaberiKamarposhti, M.; Kamyab, H.; Krishnan, S.; Yusuf, M.; Rezania, S.; Chelliapan, S.; Khorami, M.; A Comprehensive Review of AI-Enhanced Smart Grid Integration for Hydrogen Energy: Advances, Challenges, and Future Prospects. *Int. J. Hydrogen Energy* **2024**, *67*, 1009–1025.

(10) Boyano, A.; Blanco-Marigorta, A. M.; Morosuk, T.; Tsatsaronis, G. Exergoenvironmental Analysis of a Steam Methane Reforming Process for Hydrogen Production. *Energy* **2011**, *36* (4), 2202–2214.

(11) Muradov, N. Low to Near-Zero CO_2 Production of Hydrogen from Fossil Fuels: Status and Perspectives. *Int. J. Hydrogen Energy* **2017**, *42* (20), 14058–14088.

(12) Krushinski, L. E.; Dick, J. E. Direct Electrochemical Evidence Suggests That Aqueous Microdroplets Spontaneously Produce Hydrogen Peroxide. *Proc. Natl. Acad. Sci.* **2024**, *121* (12), No. e2321064121.

(13) Pradeep, T. Microdroplet Mechanochemistry. *ACS Sustainable Chem. Eng.* **2025**, *14* (1), 25–30.
(14) Xue, L.; Zheng, B.; Sun, J.; Liu, J.; Cheng, H. Water Microdroplet Chemistry for Accelerating Green Thiocyanation and Discovering Water-Controlled Divergence. *ACS Sustainable Chem. Eng.* **2023**, *11* (34), 12780–12789.
(15) Zhu, X.; Zhang, W.; Lin, Q.; Ye, M.; Xue, L.; Liu, J.; Wang, Y.; Cheng, H. Direct Microdroplet Synthesis of Carboxylic Acids from Alcohols by Preparative Paper Spray Ionization without Phase Transfer Catalysts. *ACS Sustainable Chem. Eng.* **2019**, *7* (7), 6486–6491.
(16) Wei, Z.; Li, Y.; Cooks, R. G.; Yan, X. Accelerated Reaction Kinetics in Microdroplets: Overview and Recent Developments. *Annu. Rev. Phys. Chem.* **2020**, *71* (1), 31–51.
(17) Yan, X.; Bain, R. M.; Cooks, R. G. Organic Reactions in Microdroplets: Reaction Acceleration Revealed by Mass Spectrometry. *Angew. Chem., Int. Ed.* **2016**, *55* (42), 12960–12972.
(18) Kulyk, D. S.; Miller, C. F.; Badu-Tawiah, A. K. Reactive Charged Droplets for Reduction of Matrix Effects in Electrospray Ionization Mass Spectrometry. *Anal. Chem.* **2015**, *87* (21), 10988–10994.
(19) Heiss, D. R.; Badu-Tawiah, A. K. In-Source Microdroplet Derivatization Using Coaxial Contained-Electrospray Mass Spectrometry for Enhanced Sensitivity in Saccharide Analysis. *Anal. Chem.* **2021**, *93* (50), 16779–16786.
(20) Lee, J. K.; Walker, K. L.; Han, H. S.; Kang, J.; Prinz, F. B.; Waymouth, R. M.; Nam, H. G.; Zare, R. N. Spontaneous Generation of Hydrogen Peroxide from Aqueous Microdroplets. *Proc. Natl. Acad. Sci.* **2019**, *116* (39), 19294–19298.
(21) Martins-Costa, M. T. C.; Ruiz-López, M. F. The Effect of Electric Fields on Oxidization Processes at the Air-Water Interface. *Angew. Chem., Int. Ed.* **2024**, *64* (6), No. e202418593.
(22) Chen, B.; Xia, Y.; He, R.; Sang, H.; Zhang, W.; Li, J.; Chen, L.; Wang, P.; Guo, S.; Yin, Y.; Hu, L.; Song, M.; Liang, Y.; Wang, Y.; Jiang, G.; Zare, R. N. Water–Solid Contact Electrification Causes Hydrogen Peroxide Production from Hydroxyl Radical Recombination in Sprayed Microdroplets. *Proc. Natl. Acad. Sci.* **2022**, *119* (32), No. e2209056119.
(23) Asserghine, A.; Baby, A.; N'Diaye, J.; Romo, A. I. B.; Das, S.; Litts, C. A.; Jain, P. K.; Rodríguez-López, J. Dissolved Oxygen Redox as the Source of Hydrogen Peroxide and Hydroxyl Radical in Ultrasonicated Emulsive Water Microdroplets. *J. Am. Chem. Soc.* **2025**, *147* (14), 11851–11858.
(24) Chen, F.; Wu, J.; Wang, D.; Xia, Y.; Song, Q.; Liang, Y.; Wang, P.; Chen, B.; Liang, Y.; Yin, Y.; Wang, Y.; Song, M.; Jiang, G. Simultaneous Generation of Hydroxyl and Hydrogen Radicals from H^+ /OH^- Pairs Caused by Water–Solid Contact Electrification. *Chem. Sci.* **2024**, *15* (46), 19583–19587.
(25) Das, S.; Zhou, Y.; Croslow, S. W.; Li, S.; Kim, D. O.; Santiago-Carboney, A.; Huang, S.; Nguyen, H. V.; Schroeder, C. M.; Sweedler, J. V.; Assary, R. S.; Moore, J. S.; Rodríguez-López, J. One-Step, High-Yield Deconstruction of Kraft Lignin into a Redox-Active Small Molecule Using Ultrasonicated Emulsive Water Microdroplets. *ChemRxiv* **2025**.
(26) Song, X.; Basheer, C.; Xia, Y.; Li, J.; IsmailAbdulazeez; Al-Saadi, A. A.; Mofidfar, M.; Suliman, M. A.; Zare, R. N. One-Step Formation of Urea from Carbon Dioxide and Nitrogen Using Water Microdroplets. *J. Am. Chem. Soc.* **2023**, *145* (47), 25910–25916.
(27) Meng, Y.; Xia, Y.; Xu, J.; Zare, R. N. Spraying of Water Microdroplets Forms Luminescence and Causes Chemical Reactions in Surrounding Gas. *Sci. Adv.* **2025**, *11* (11), No. eadt8979.
(28) Zhang, J.; Liu, Z.; Zhu, C.; Wang, S.; Zhu, S.; Zhu, C.; Zhang, X. Ion-Specific Interfacial Electric Fields on Water Microdroplets for Tuning Menshutkin Reactions. *J. Am. Chem. Soc.* **2025**, *147* (42), 38428–38434.
(29) Song, X.; Jallow, J.; Basheer, C.; Bakdash, R. S.; Alaliwi, A.; Alzamil, A. A.; Zare, R. N. Microdroplet-Driven Synthesis of a Metal–Organic Framework Catalyst. *Angew. Chem., Int. Ed.* **2025**, *64*, No. e202515006.
(30) Nguyen, D.; Lyu, P.; Nguyen, S. C. Experimental and Thermodynamic Viewpoints on Claims of a Spontaneous H_2O_2 Formation at the Air–Water Interface. *J. Phys. Chem. B* **2023**, *127* (11), 2323–2330.
(31) Eatoo, M. A.; Mishra, H. Busting the Myth of Spontaneous Formation of H2O2 at the Air–Water Interface: Contributions of the Liquid–Solid Interface and Dissolved Oxygen Exposed. *Chem. Sci.* **2024**, *15*, 3093–3103.
(32) LaCour, R. A.; Heindel, J. P.; Zhao, R.; Head-Gordon, T. The Role of Interfaces and Charge for Chemical Reactivity in Microdroplets. *J. Am. Chem. Soc.* **2025**, *147* (8), 6299–6317.
(33) Eatoo, M. A.; Mishra, H. Disentangling the Roles of Dissolved Oxygen, Common Salts, and PH on Spontaneous Hydrogen Peroxide Production in Water: No O_2, No H_2O_2. *J. Am. Chem. Soc.* **2025**, *147* (39), 35392–35400.
(34) Li, F.; Lv, J.; He, A.; Xu, J.; Zhao, L.; Wang, X.; Mao, L.; Li, S.; Wang, H.; Wang, Y.; Jiang, G. Unexpected Generation of Singlet Oxygen at the Air–Water Interface of Aqueous Microdroplets. *J. Am. Chem. Soc.* **2025**, *147* (34), 30574–30581.
(35) Chen, X.; Xia, Y.; Zhang, Z.; Lee, H.; Jia, X.; Wang, F.; Zare, R. N. Hydrocarbon Degradation by Contact with Anoxic Water Microdroplets. *J. Am. Chem. Soc.* **2023**, *145* (39), 21538–21545.
(36) Chen, S.; Li, X.; Fang, Y.-G.; Liu, X.; Yao, Y.; Chen, B.; Francisco, J. S.; Zhu, C.; Chu, C. Accelerated Fatty Acid Oxidation Occurs at the Water–Air Interface of Sea Spray Microdroplets. *J. Am. Chem. Soc.* **2025**, *147* (42), 38609–38614.
(37) He, Y.; Xu, J.; Lyu, L.; Xia, Y.; Zare, R. N.; Meng, Y. Water Droplet Microlightning Enables Catalyst-Free Alkane Dehydrogenation under Ambient Conditions. *ACS Sustainable Chem. Eng.* **2026**, *14* (15), 7092–7098.
(38) U.S. Department of Agriculture, Foreign Agricultural Service. In *Production – Palm Oil*. https://www.fas.usda.gov/data/production/commodity/4243000 (accessed July 25, 2026).
(39) Morhart, T. A.; Unni, B.; Lardner, M. J.; Burgess, I. J. Electrochemical ATR-SEIRAS Using Low-Cost, Micromachined Si Wafers. *Anal. Chem.* **2017**, *89* (21), 11818–11824.
(40) Siddiqui, A.-R.; N'Diaye, J.; Martin, K.; Baby, A.; Dawlaty, J.; Augustyn, V.; Rodríguez-López, J. Monitoring SEIRAS on a Graphitic Electrode for Surface-Sensitive Electrochemistry: Real-Time Electrografting. *Anal. Chem.* **2024**, *96* (6), 2435–2444.
(41) Merabet, N.; Kerboua, K. Sonolytic and Ultrasound-Assisted Techniques for Hydrogen Production: A Review Based on the Role of Ultrasound. *Int. J. Hydrogen Energy* **2022**, *47* (41), 17879–17893.
(42) Suslick, K. S.; Gawienowski, J. J.; Schubert, P. F.; Wang, H. H. Alkane Sonochemistry. *J. Phys. Chem.* **1983**, *87* (13), 2299–2301.
(43) Lee, K.; Cho, Y.; Kim, J. C.; Choi, C.; Kim, J.; Lee, J. K.; Li, S.; Kwak, S. K.; Choi, S. Q. Catalyst-Free Selective Oxidation of $C(sp^3)$-H Bonds in Toluene on Water. *Nat. Commun.* **2024**, *15* (1). No. 6127.
(44) Zhou, X.; Du, S.; Zhang, W.; Zheng, B. Deciphering the Mechanism of Hydrogen Peroxide Formation in Ultrasound-Mediated Water-In-Oil Microdroplets. *Chem. Sci.* **2025**, *16* (15), 6450–6457.
(45) Mortimer, C. H. The oxygen content of air-saturated fresh waters, and aids in calculating percentage saturation: With 2 tables and 5 figures in the text. *Internationale Vereinigung für Theoretische und Angewandte Limnologie: Mitteilungen* **1956**, *6* (1), 1–20.
(46) Xing, W.; Yin, M.; Lv, Q.; Hu, Y.; Liu, C.; Zhang, J. Oxygen Solubility, Diffusion Coefficient, and Solution Viscosity. *Rotating Electrode Methods and Oxygen Reduction Electrocatalysts* **2014**, 1–31.
(47) Chen, Y.-F.; Chu, L.-K. Infrared Characterization of Isotopic Analogues of Methanediol in Aqueous Solution. *J. Phys. Chem. A* **2022**, *126* (32), 5302–5309.
(48) Joseph, J. M.; Destaillats, H.; Hung, H.-M.; Hoffmann, M. R. The Sonochemical Degradation of Azobenzene and Related Azo Dyes: Rate Enhancements via Fenton's Reactions. *J. Phys. Chem. A* **1999**, *104* (2), 301–307.
(49) Price, G. J.; McCollom, M. The Effect of High-Intensity Ultrasound on Diesel Fuels. *Ultrason. Sonochem.* **1995**, *2* (2), S67–S70.
(50) Xia, D.; Xie, H.; Fu, Z.; Chen, J. Microdroplets: An Overlooked "Engine" of Chemistry in Air. *Environ. Sci. Technol.* **2025**. *59*, 6357.

(51) He, Y.; Zhao, J.; Sham, Y.-T.; Gao, S.; Pan, M.; Chen, Q.; Huang, G.; Wong, P. K.; Bi, J. Efficient Hydrogen Peroxide Photosynthesis over CdS/COF for Water Disinfection: The S-Scheme Pathway, Oxygen Adsorption, and Reactor Design. *ACS Sustainable Chem. Eng.* **2023**, *11* (49), 17552–17563.
(52) Meroni, D.; Djellabi, R.; Ashokkumar, M.; Bianchi, C. L.; Boffito, D. C. Sonoprocessing: From Concepts to Large-Scale Reactors. *Chem. Rev.* **2021**, *122* (3), 3219–3258.
(53) Merouani, S.; Dehane, A.; Hamdaoui, O. Ultrasonic Decomposition of Endocrine Disrupting Compounds – A Review. *Ultrason. Sonochem.* **2024**, *110*, No. 107026.
(54) Manickam, S.; Boffito, D. C.; Flores, E. M.; Lévêque, J. M.; Pflieger, R.; Pollet, B. G.; Ashokkumar, M. Ultrasonics and Sonochemistry: Editors' Perspective. *Ultrason. Sonochem.* **2023**, *99*, No. 106540.

https://doi.org/10.1021/acssuschemeng.6c05673
ACS Sustain. Chem. Eng. 2026, 14, 15850–15862